Design of a single-stage collector for a hollow-beam klystron

Stanley Humphries, Ph.D.

Field Precision LLC
E mail: techinfo@fieldp.com
Internet: https://www.fieldp.com

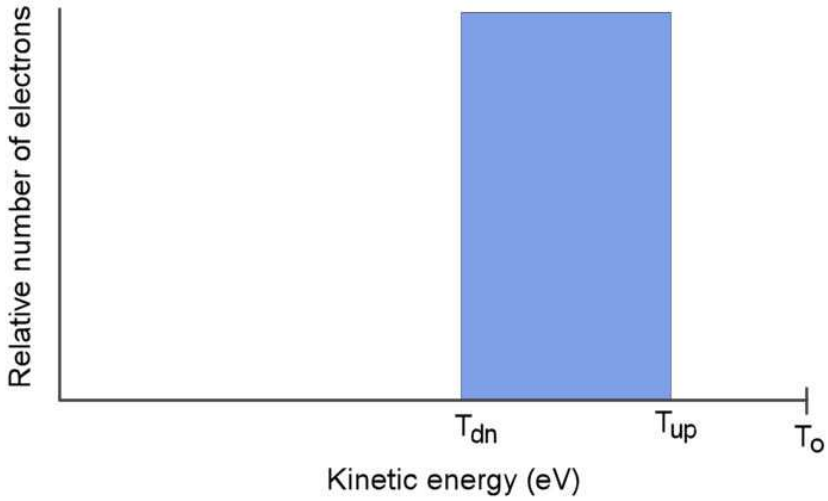

Figure 1: Simplified energy distribution for an electron beam emerging from a klystron.

1 Dynamics of a single-stage collector

The tutorial reviews constraints on the performance of a single-stage biased collector to improve the energy efficiency of a hollow-beam klystron system[1]. It also describes design studies for a collector. If the exit beam from a klystron were monoenergetic, it would be possible to recover the full energy in a biased collector. Tradeoffs are necessary when the beam has an energy spread. Increasing the efficiency of the RF device results in reduced energy and increased dispersion in the exit beam. In a real system, the performance of the tube and the collector must be balanced to optimize the system. There is a potentially large parameter space to explore.

I will present a simplified models to gain some insight into realistic goals and performance optimization. I assume that beam emerging from klystron has the idealized kinetic energy distribution show in Fig. 1. The electrons have a uniform distribution of kinetic energy from T_{dn} to T_{up}. The quantity T_o is the injection kinetic energy. Further, I assume that there is no electron loss or resistive energy dissipation in the klystron. so that the kinetic energy loss from beam appears as RF energy. In this case, the RF energy produced per electron is:

[1]The electron gun for the klystron case study is described in the tutorial **Electron Gun Design for a Hollow-beam Klystron using Trak**. The focusing magnetic design is reviewed in the tutorial **PerMag Design of a Focusing Magnet for a Hollow-beam Klystron**.

$$E_{rf} = T_o - \frac{T_{up} + T_{dn}}{2}. \tag{1}$$

Equation 1 can be written in the normalized form:

$$e_{rf} = \frac{E_{rf}}{T_o} = 1 - \frac{t_{up} + t_{dn}}{2}. \tag{2}$$

where $t_{up} = T_{up}/T_o$ and $t_{dn} = T_{dn}/T_o$.

The quantity T_c is the electron kinetic energy associated with the collector voltage, $T_c = -eV_c$. The energy per electron recovered in the collector depends on the value of T_c compared to the limits of the beam energy distribution:

$$E_c = 0.0, \qquad (T_c > T_{up}) \tag{3}$$

$$E_c = \left(\frac{T_{up} - T_c}{T_{up} - T_{dn}}\right) T_c, \qquad (T_{dn} < T_c < T_{up}) \tag{4}$$

$$E_c = T_c, \qquad (T_c < T_{dn}) \tag{5}$$

In Eq. 4, the quantity in parenthesis in the fraction of electrons that can enter the collector at the bias level T_c. The remainder are presumed lost at the collector entrance. A practical collector must run in the regime described by Eq. 4. The condition of Eq. 3 implies that all electrons are rejected and the collector serves no purpose. In the range of Eq. 5, all electrons are collected but recovered energy is wasted by running at a low bias voltage.

Defining the normalized variable $t_c = T_c/T_o$, the normalized recovered energy per electron is:

$$e_c = \left(\frac{t_{up} - t_c}{t_{up} - t_{dn}}\right) t_c. \tag{6}$$

Adding Eqs. 2 and 6, the normalized energy utilized per electron is

$$e = 1 - \frac{t_{up} + t_{dn}}{2} + \left(\frac{t_{up} - t_c}{t_{up} - t_{dn}}\right) t_c. \tag{7}$$

To begin we address the following question: for given values of t_{up} and t_{dn}, what choice of t_c gives the highest energy recovery fraction? Taking the derivative of Eq. 7 and setting $de/dt_c = 0$, we find that:

$$t_c = \frac{t_{up}}{2}, \tag{8}$$

when $t_{up}/2 < t_{dn}$. If $t_{up}/2 > t_{dn}$, then the best choice of normalized collector voltage is $t_c = t_{dn}$.

Table 1: Normalized energy recovery, $\Delta t = 0.25$.

t_{up}	t_c	e_{RF}	e_c	e
1.000	0.750	0.125	0.750	0.875
0.900	0.650	0.225	0.650	0.875
0.800	0.550	0.325	0.550	0.875
0.700	0.450	0.425	0.450	0.875
0.600	0.350	0.525	0.350	0.875
0.500	0.350	0.625	0.250	0.875
0.400	0.200	0.725	0.160	0.885
0.300	0.150	0.825	0.090	0.915
0.250	0.125	0.875	0.062	0.937

Table 2: Normalized energy recovery, $\Delta t = 0.50$.

t_{up}	t_c	e_{RF}	e_c	e
1.000	0.500	0.250	0.500	0.750
0.900	0.450	0.350	0.405	0.755
0.800	0.400	0.450	0.320	0.770
0.700	0.350	0.550	0.245	0.795
0.600	0.300	0.650	0.180	0.830
0.500	0.250	0.750	0.125	0.875

To investigate different parameter regimes, it is useful to introduce the variable $\Delta t = t_{up} - t_{dn}$ in Eqs. 2, 6 and 7:

$$e_{rf} = 1 - t_{up} + \Delta t/2. \tag{9}$$

$$e_c = \left(\frac{t_{up} - t_c}{\Delta t}\right) t_c. \tag{10}$$

$$e = 1 - t_{up} + \Delta t/2 + \left(\frac{t_{up} - t_c}{\Delta t}\right) t_c. \tag{11}$$

Calculated values of recovered energy fractions as a function of t_{up} using above equations are listed in Tables 1, 2 and 3 for the choices $\Delta t = 0.25$, 0.50 and 0.75. The tabulated ranges of t_{up} are the maximum allowed consistent with the choice of Δt and the assumption that is no beam loss within klystron.

Table 3: Normalized energy recovery, $\Delta t = 0.75$.

t_{up}	t_c	e_{RF}	e_c	e
1.000	0.500	0.375	0.375	0.750
0.950	0.475	0.425	0.338	0.763
0.900	0.450	0.475	0.304	0.779
0.850	0.425	0.525	0.271	0.796
0.800	0.400	0.575	0.240	0.815
0.750	0.375	0.625	0.211	0.836

Some conclusions follow from an inspection of the tables:

There are two reasons to choose the lowest possible value of t_{up}. First, the net efficiency is higher. Second, the value corresponds to the highest RF power production for a given beam power.

The maximum value of system efficiency decreases with increasing Δt.

At the highest efficiency, the contribution of the collector increases with increasing Δt.

The theoretical efficiency is high even for exit beams with large energy spread. Therefore, we can not expect dramatic improvements for collectors with multiple bias levels. The gain may not be worth the added complexity of mechanical and electrical systems.

In this tutorial, I limit consideration to collectors with a single bias voltage.

2 Beam extraction to the collector

The collector is placed at a position of reduced magnetic field magnitude in the exit region of the solenoid. There are two reasons for the approach: 1) the cross-section area of the annular beam increases as it follows the expanding magnetic field lines, reducing power density and 2) some of the transverse energy of the electrons is converted to longitudinal energy.

The operation of a depressed collector clearly involves electrostatic optics. One issue is whether to mix magnetic forces with electric forces. The mixed-field approach was taken in Refs. [1] and [2]. After trying several calculations, I found the two reasons to avoid magnetic fields in the collector region:

> It is difficult, if not impossible, to ensure that all primary electrons with kinetic energy above T_c are collected and lower energy electrons are absorbed with no reflection.
>
> The magnetic field lines provide a conduit to guide reflector and secondary electrons back into the klystron.

I decided to place the collector inside a magnetic shield where electron motion would be governed solely by electrostatic forces. In this way, I could divide the beam extraction issue into two manageable parts:

> Propagation of electron beam along the exit region of the solenoid into the collector magnetic shield.
>
> The motion of different energy grounds of electrons inside the collector.

In this section, I discuss magnetic field configuration of a shielded collector and the issue of beam propagation. The following section covers a point design for a collector.

The magnet described in Report 04 will be used as a basis for the exit field calculations. I used the same geometry for the iron output flange (1.00" thick with 12.50" aperture radius). I added iron plates of thickness 0.75" to define a region almost free of magnetic fields for the electrostatic collector. Figure 2 shows the geometry. There was some latitude in the choice of collector dimensions. The annular shield has same inner and outer radii as the output plate and a length such that the total collector length (defined as the distance from the end of uniform field region at $z = 60.00$" to the end of the collector structure) is less than 30". Field lines are included on the left-hand side of Fig. 2. I found that the shield had a negligible effect on the field configuration inside the klystron. Field lines in the beam transport region intersect the collector entrance at a right angle. Because electrons are tied to field lines, the beam motion should be radial at the collector entrance,

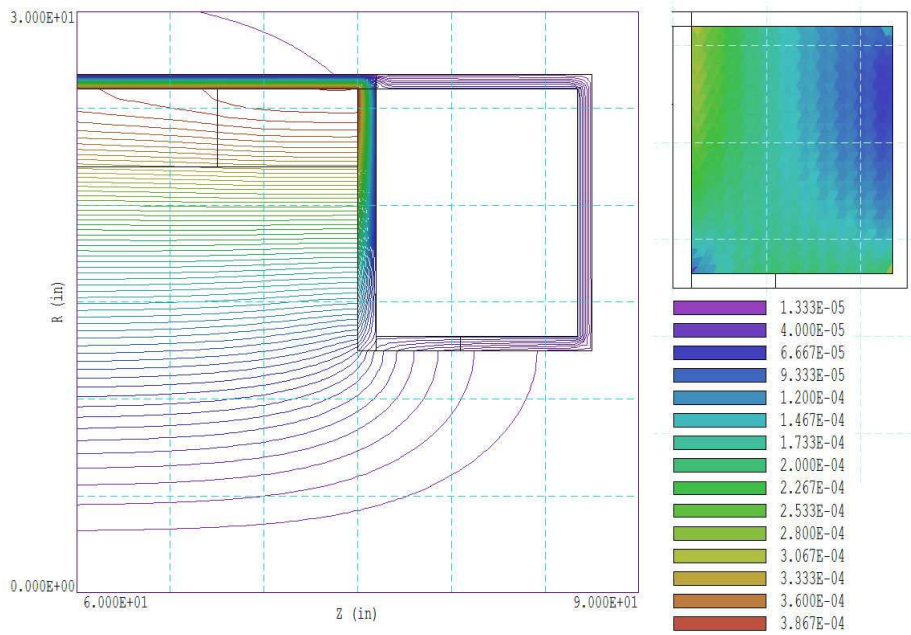

Figure 2: Magnetic field in the solenoid region with a shielded box added for the collector. The left-hand side shows magnetic field lines, while the right-hand side shows $|\mathbf{B}|$ inside the box.

an advantage for a compact collector design. The right-hand side of Fig. 2 shows that $|\mathbf{B}|$ inside the shield is less than 2.8 G at all positions.

The following tasks were performed to complete the study:

1. Find the position where the beam strikes the shield box and introduce an entrance aperture.

2. Generate a distribution that approximate the expected exit beam from the hollow-beam klystron.

3. Propagate the electrons out of the solenoid and ensure that entire beam enters the aperture.

4. Find characteristics of the beam entering the shield box to use in calculations of the following section.

The injected beam described in Report 02 has a small radial oscillation and fills a region from about $r_i = 5.25$" to $r_o = 5.50$". To locate the approximate intersection point of beam, I found the corresponding values of rA_θ in the uniform-field region (8.92×10^{-4} tesla-m^2 to 9.79×10^{-4} tesla-m^2). A plot of the corresponding stream function contours shows the approximate limits of the beam envelope. The top of Fig. 3 shows the result. I added an aperture

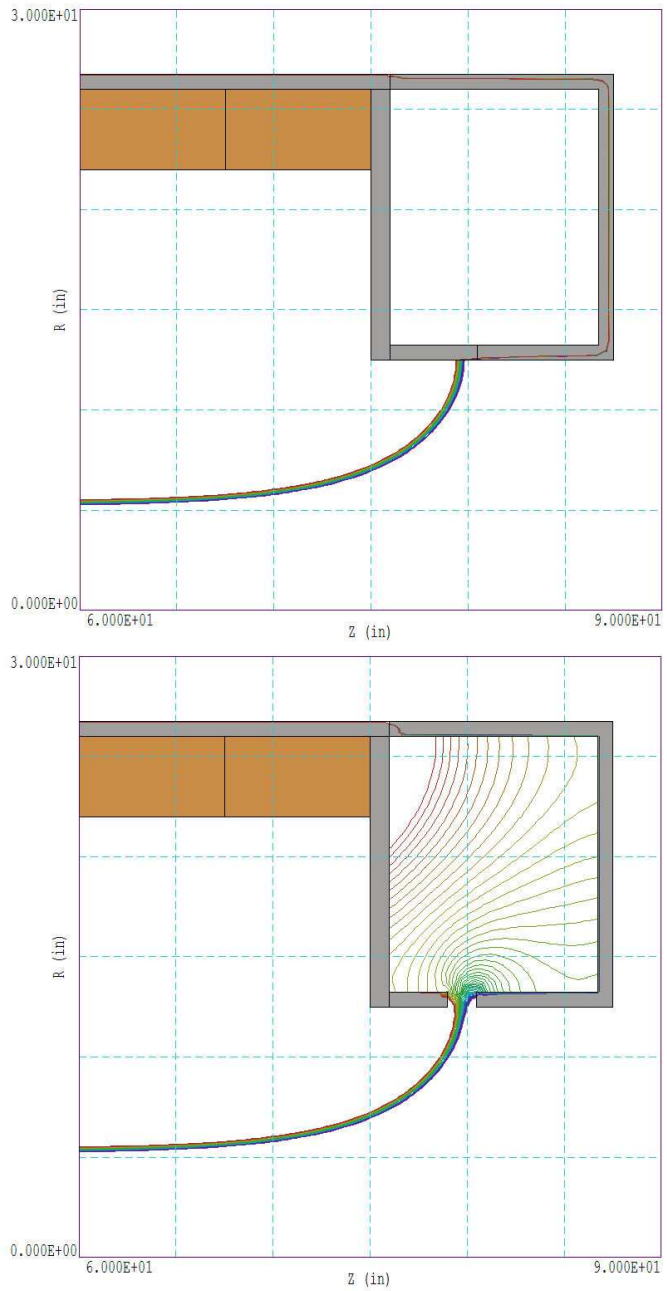

Figure 3: Plot of magnetic fields (contours of rA_θ) corresponding to the inner and outer radii of the annular beam in uniform-field region. Top: ideal shield. Bottom: shield with aperture.

centered at the intersection position of axial width 1.00". The resulting field lines are shown at the bottom of Fig. 3. (Note that the lines inside the shield region exaggerate the internal field because of small range of rA_θ.) Although the field penetrates through the aperture a distance comparable to its axial width, the field level over most of internal volume is less than 3 G.

To investigate electron propagation into the shielded collector, it was necessary to generate distribution representative of that from a high-efficiency klystron. I added a feature to the **GenDist** program to handle annular beams. To check the worst possible case, I considered a strongly-perturbed beam: a radial width of 0.75"with large spreads in direction and kinetic energy. The **GenDist** input file (reproduced in Table 4) creates 500 model electrons. The `DEF CIRC` and `RDIST` commands set a uniform distribution of electrons in the radius range 5.00"$\leq r \leq$5.75". The `ENERGY` and `TDIST` commands defined a uniform distribution in energy from 10.0 keV to 65.0 keV. Finally, the `DXDIST` and `DYDIST` structures give an angular divergence of $\pm 5.0^{\circ}$ in the r and θ directions. I initiated the beam at the end of the uniform-field region (z = 60.0") with a Neumann condition on upstream boundary.

I used the input distribution in a **Trak** simulation of beam propagation that included effects of space charge and beam-generated magnetic fields. It was necessary to include an electrostatic solution to determine the beam-generated potential. I assumed a 6.00" drift tube that expanded to contact the inner radius of the iron output plate. All parts of the magnetic shield were at ground potential.

Because of the broad initial radial beam width combined with beam expansion in the fringe magnetic field, it was necessary to increase the axial width of the entrance slot to 1.75". I also moved it downstream about 0.25" because the electrons were not tied perfectly to the field lines. Figure 4 plots the electron orbits and the beam-generated electrostatic potential. The full beam current enters the shield chamber. Here, the electrons expand freely in the absence of magnetic confining force. The figure shows a spread of angles in the z direction of about $\pm 20^{\circ}$. Figure 5 shows a projection of the orbits in the x-y plane. (Although space-charge assignment in **Trak** is symmetric in θ, model orbits are calculated in x-y-z space.) All orbits start in plane $y = 0.0$", but immediately spread because of assigned azimuthal angular divergence. This is followed by a slower spread as the electrons move out of the solenoid into weak field region. and then free expansion in the shield chamber. The envelope for angular spread in the θ direction was approximately $\pm 17^{\circ}$.

Although the beam spread presents a challenge for electrostatic optics in collector, it is beneficial for the operation of the device. The beam from injector has peak power 19.17 MW. With a pulse length of 5.0×10^{-4} s and repetition rate of 15 Hz, the duty cycle is 0.0075. Therefore, the average

Table 4: File `HBKExit.DST`, input for the **GenDist** program

```
FILETYPE = PRT
RESTMASS = 0.0
CHARGE = -1.0
ENERGY = 37.0E3
CURRENT = 177.5
DEF Circ 5.25 5.50  500  1
SHIFT 0.00 0.00 60.001
DISTRIBUTION Uniform
TDIST
  -27.0E3   1.0
  -17.0E3   1.0
   -7.0E3   1.0
    0.0E3   1.0
    7.0E3   1.0
   17.0E3   1.0
   27.0E3   1.0
END
RDIST
   0.00    1.0
   0.20    1.0
   0.40    1.0
   0.60    1.0
   0.80    1.0
   1.00    1.0
END
DXDIST
  -5.00    1.0
  -2.50    1.0
   0.00    1.0
   2.50    1.0
   5.00    1.0
END
DYDIST
  -5.00    1.0
  -2.50    1.0
   0.00    1.0
   2.50    1.0
   5.00    1.0
END
ENDFILE
```

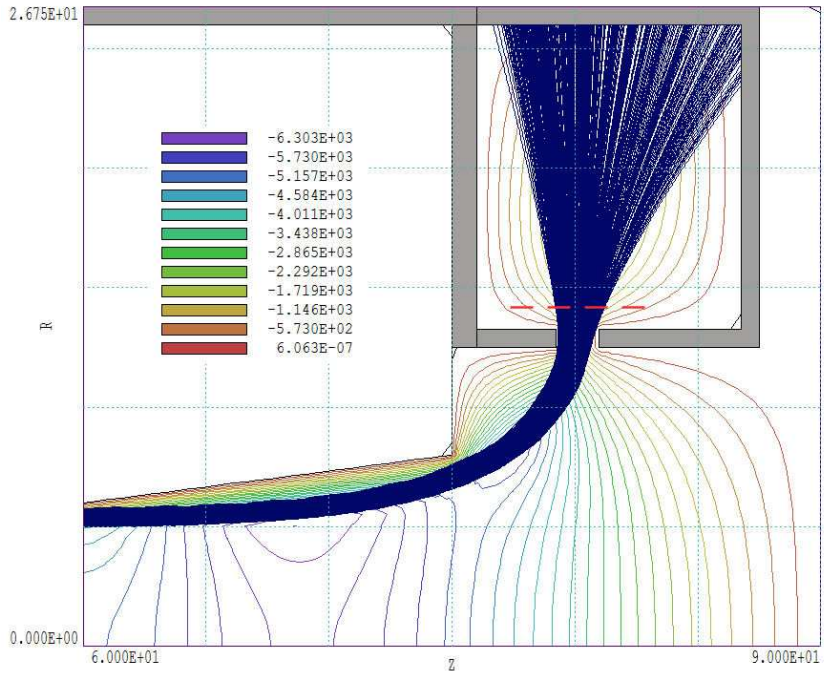

Figure 4: Plot in z-r of beam propagation out of the solenoid into the collector shield. The beam consists of 500 model electrons with a large spread in radius, kinetic energy and direction.

beam power is 143.8 kW. The cross-section area of the beam from the injector is about 46.34 cm^2. Therefore, the average beam power density from the injector is about 3.1 kW/cm^2. From the discussion of Sect. 1, less than 20% of the power will be dissipated through collisions in the collector. An inspection of Fig. 4 shows that the collector area could exceed 5000 cm^2, giving a maximum power density of about 0.078 kW/cm^2. There should be no problem with surface damage, and it should be relatively easy to design a cooling system.

3 Initial design of a single-stage collector.

This section covers an initial design of an array of electrodes in the shield chamber to recover the energy of entering electrons. As in previous section, I consider a spread of electron energy 10 keV to 65 keV. Figures 4 and 5 include particles of all energies and exaggerate the angular spread in z. I set a diagnostic plane in **Trak** to record particle parameters along the dashed red line in Fig. 4. I loaded the resulting `PRT` file into **GenDist** and applied a filter to include only electrons with kinetic energy greater than 35 keV. The

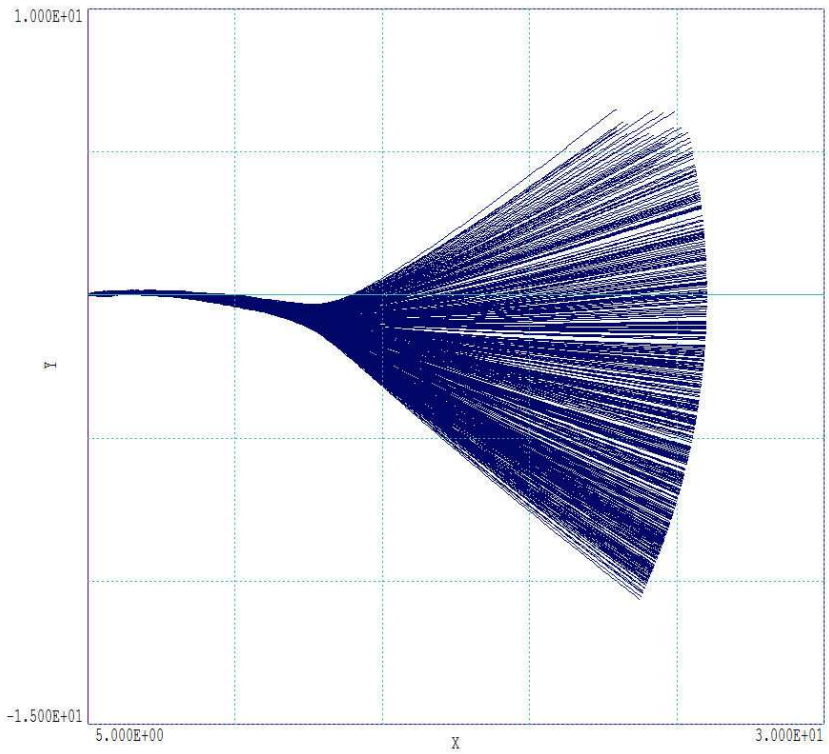

Figure 5: Projection plot in x-y of beam propagation out of the solenoid into the collector shield. The beam consists of 500 model electrons with a large spread in radius, kinetic energy and direction.

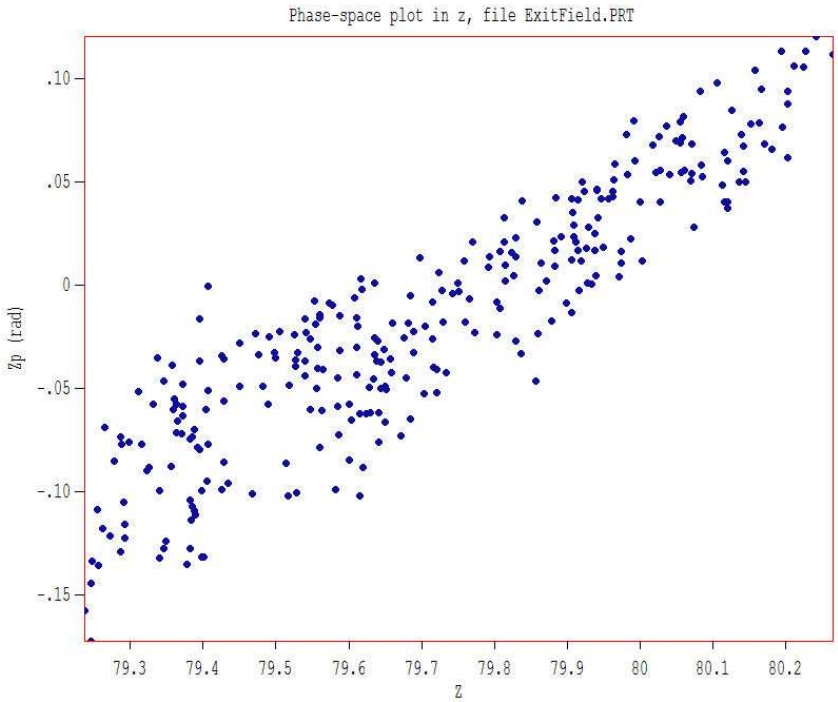

Figure 6: Phase space distribution z-z' relative to r along the dashed red line shown in Fig. 4. Filter: $T_e \geq 35.0$ keV.

resulting phase-space plot of Fig. 6 was constructed with reference axis along r. The high-energy particles had an average inclination angle along z of 1.4^o with an angular spread $\pm 7.2^o$.

Following the discussion of Sect. 1, the best collector voltage was about -35 kV. An ideal collector should have the following characteristics:

> Prevent backflow of electrons through the aperture, either by electron reflection or transport of secondary electrons created on the collector.
>
> Direct all electrons with $T_e \leq 35.0$ keV to a ground electrode at some distance from the aperture.
>
> Direct all electrons with $T_e > 35.0$ keV to the biased collector.
>
> Prevent the flow of secondary electrons from the collector surface to grounded electrodes.

Regarding backflow, it is inevitable that some electrons with kinetic energy close to the collector voltage will be reflected. The goal is to ensure that such electrons have large transverse energy. In this case, the converging magnetic

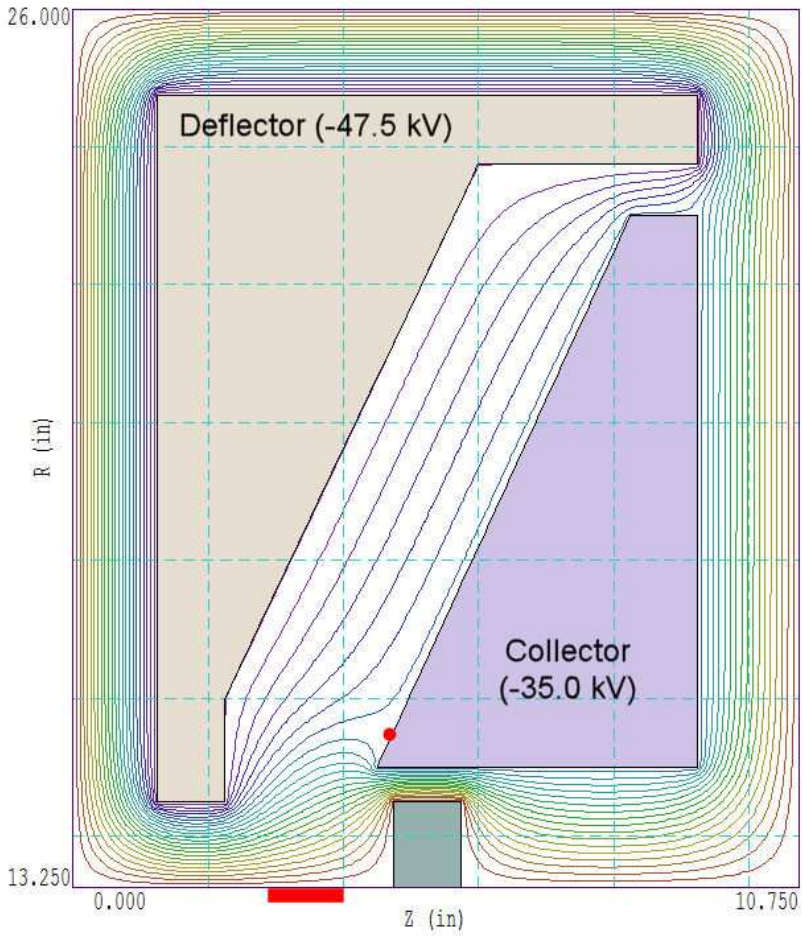

Figure 7: Collector geometry, z-r plot. Surrounding shield at ground potential. Red box shows the limits of the injected beam. The red dot shows the separatrix of the good-field region on the collector surface.

field lines at the aperture act as a magnetic mirror to inhibit electron transport.

I devised an electrode configuration that comes close to meeting the goals. Figure 7 shows the geometry and electrostatic equipotential lines. The idea is that entering electrons experience a strong transverse electric field created by a deflector electrode and an extension of the grounded wall. The field sweeps electrons downstream where most of the low-energy particles impinge on the chamber wall and ground extension. In the collection region, the electric field prevents extraction of secondaries electrons. The higher-energy electrons follow curved trajectories and impact over the large collector face. At points above the red dot in Fig. 7, the direction of the electric field ensures confinement of secondary electrons to the surface. The good-field region may be larger when the effects of the negative space-charge potential of the incoming beam are included. Note that While the collector intercepts a large fraction of the beam current, there is no current flow to the deflector. The deflector voltage can therefore be supplied by a high-impedance circuit.

The remainder of this section discusses results of **Trak** simulations using model electron distributions that reflect the discussion of Sect. 2. To begin, I assume electrons initial travel in the radial direction. Figure 8 shows trajectories of electrons with kinetic energy higher than the collector voltage ($T_e \geq 40.0$ keV). There is a spread of axial positions of of ± 0.5" relative to the center of the aperture. All orbits impinge on the collector face, spread over a radial span of about 7.5". Only one model electron strikes the collector surface in a region when secondaries could be extracted.

The top portion of Figure 9 shows orbits with injection energy in the range of the collector voltage (30, 35 and 40.0 keV). Lower energy electrons are stopped on the ground extension while higher energy electrons reach the collector. Two electrons with kinetic energy exactly equal to collector voltage follow orbits that return them to the aperture. A goal of following optimization studies would be to check whether such orbits can propagate back into the rising field and whether it is possible to modify electrodes to reduce electron reflection. The bottom section of Fig. 9 shows trajectories of low-energy electrons in the range 10-30 keV. Most are collected on the ground extension while a few may re-enter aperture at a displaced location with high transverse energy. Finally, Fig. 10 shows trajectories of electrons in energy range 40-65 keV with both spatial displacements and angular divergence. Only a few fraction does not reach the good-field region of the collector. In conclusion, it appears that all electrons in the exit beam of the hollow-beam klystron can be transported into a magnetic shield. A point design shows that electrostatic fields can effectively sort particles by energy and spread them out for collection at low power density. The performance is close to the theoretical limits discussed in Sect. 1.

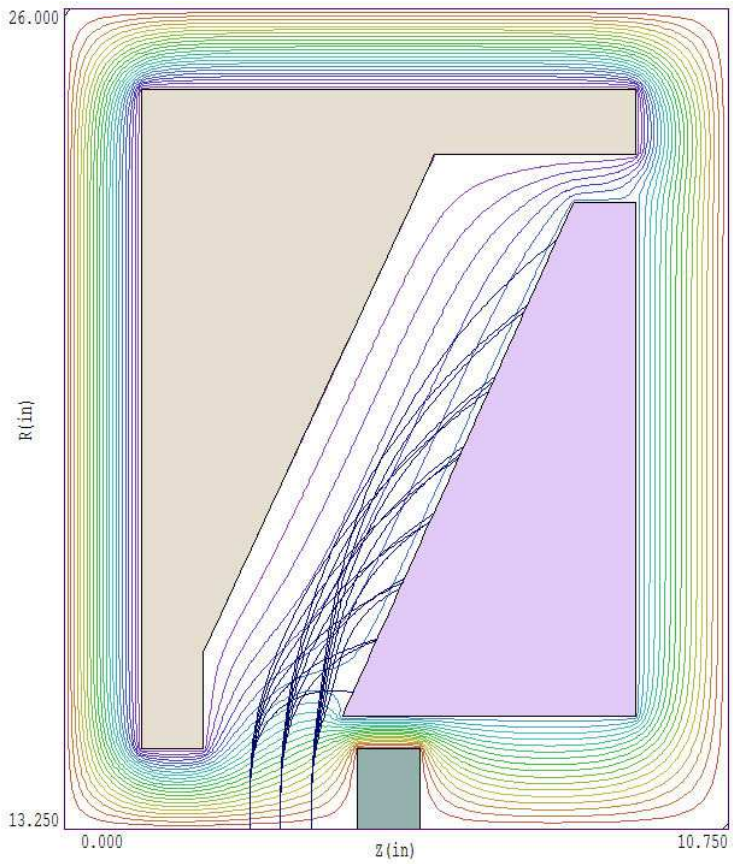

Figure 8: Trajectories of high-energy electrons, started parallel to r direction at positions $\Delta z = -0.5$", 0.0" and 0.5"with respect to the aperture center. Energies: 40.0, 45.0, 55.0, 60.0 and 65.0 keV.

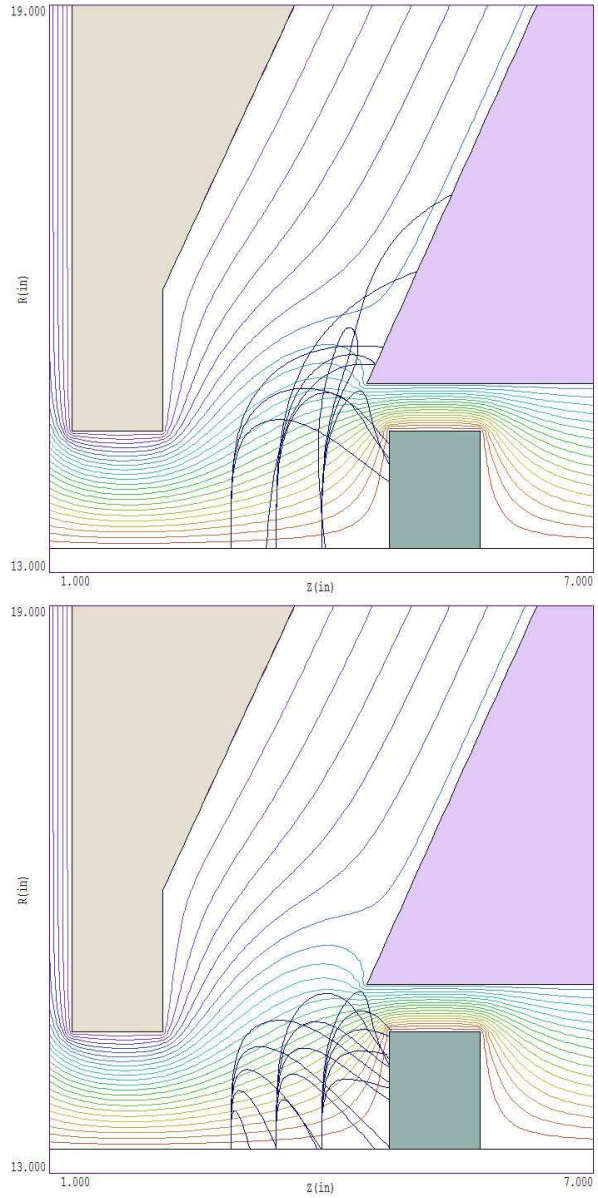

Figure 9: Trajectories of medium and low energy electrons, started parallel to r direction at positions $\Delta z = -0.5$", 0.0" and 0.5"with respect to the aperture center. Energies in top illustration: 30.0, 35.0 and 40.0 keV. Energies in bottom illustration: 10.0, 15.0, 20.0, 25.0 and 30.0 keV.

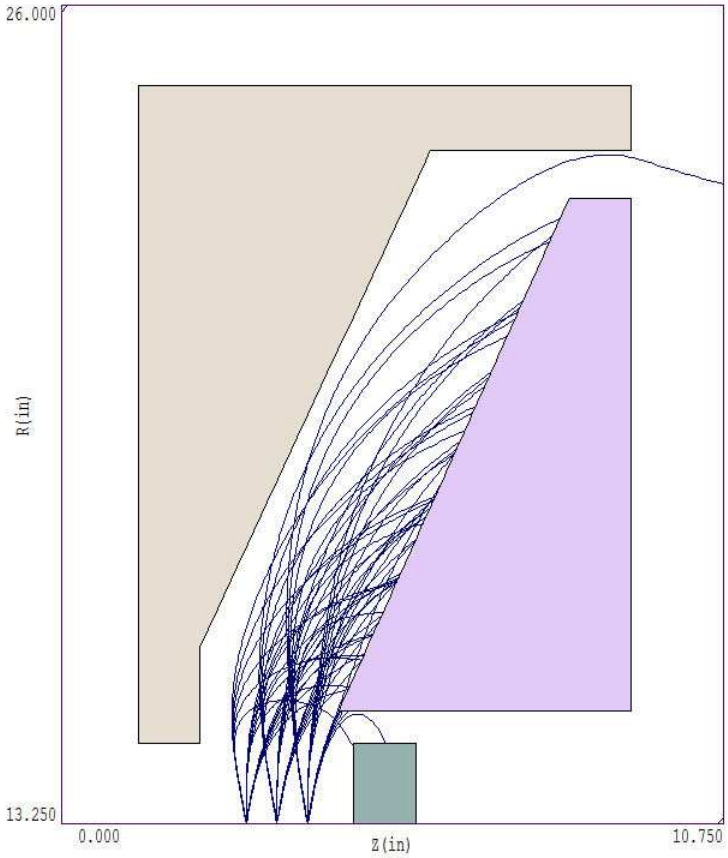

Figure 10: Trajectories of high-energy electrons with a spread in position with respect to the aperture center ($\Delta z = \pm 0.5$") and angle with respect to r ($\Delta z' = \pm 10.0^{o}$). Energies: 40.0, 45.0, 55.0, 60.0 and 65.0 keV.

References

[1] A. Singh, S. Rajapatirana, Y. Men, V. Granatstein, R. Ives and A. Antolak, *Design of a multistage depressed collector system for 1-MW CW gyrotrons – Part I: Trajectory controls of primary and secondary electrons in a two-stage depressed collector*, IEEE Trans. Plasma Sci. **27** (1999), 490.

[2] R. Ives , A. Singh, M. Mizuhara, R. Schumacher, J. Neilson, M. Gandreau, J. Casey and V. Granatstein, D*esign of a multistage depressed collector system for 1-MW CW gyrotrons – Part II: System consideration*, IEEE Trans. Plasma Sci. **27** (1999), 503.